Journal of Bio- and Tribo-Corrosion (2019) 5:21
https://doi.org/10.1007/s40735-018-0215-3

Corrosion Inhibition of Ordinary Steel in 5.0 M HCl Medium by Benzimidazole Derivatives: Electrochemical, UV–Visible Spectrometry, and DFT Calculations

O. Fergachi[1] · F. Benhiba[5] · M. Rbaa[2] · M. Ouakki[3] · M. Galai[1] · R. Touir[4] · B. Lakhrissi[2] · H. Oudda[5] · M. Ebn Touhami[1]

Received: 30 August 2018 / Revised: 24 November 2018 / Accepted: 19 December 2018 / Published online: 3 January 2019

Abstract
In the present work, a new organic inhibitor, namely (2(-4(chloro phenyl-1*H*-benzo[d]imidazol)-1-yl)phenyl) methanone (CBIPM), that has an inhibitive effect on the ordinary steel corrosion in 5.0 M HCl has been studied using electrochemical measurements (potentiodynamic polarization and electrochemical impedance spectroscopy). The obtained results showed that the inhibition efficiency increased with concentration and reached 98.6% at 10^{-3} M. In addition, the CBIPM takes its performance at the temperature range of 298–328 K. The adsorption of the inhibitor on the ordinary steel was well described by the Langmuir isotherm. On the other hand, the establishing of correlation between the molecular structures of quantum chemistry indices was carried out using the density functional theory.

Keywords Imidazol · Ordinary steel · Corrosion inhibition · Acidic medium · UV–visible spectroscopy · DFT

1 Introduction

The importance of protection against corrosion in acidic solutions has been increased by the fact that iron materials, which are more susceptible to be attacked in aggressive media, are the commonly exposed metals in industrial environments. Hydrochloric acid, for example, is often used as a pickling acid for iron and its alloys to remove undesirable corrosion products. The chemical acid cleaning will cause metal corrosion upon the already cleaned surface after the elimination of the corrosion products. Corrosion inhibitors efficiently reduce the undesirable destructive effect and prevent metal dissolution [1].

Acid inhibitors are essentially used in metal finishing industries, acidizing of oil wells, cleaning of boilers, and heat exchangers. The efficiency of an inhibitor is largely dependent on its adsorption on the metal surface, which consists of replacement of humidity by the organic inhibitor [2]. Most well-known inhibitors are organic compounds containing hetero atoms such as nitrogen, sulfur, and/or oxygen atoms [3, 4]. In addition, many *N*-heterocyclic compounds have been demonstrated as effective inhibitors against corrosion of metals and alloys in acid solutions [5–7]. The use of organic compounds as inhibitors is one of the most widely used methods for protecting materials from corrosion [8, 9]. Recently, many workers have reoriented their attention to the development of new corrosion inhibitors based on organic compounds such as imidazopyridine [10], imidazole [11, 12], Triazepine Carboxylate [13], and tetrazole [14, 15]. Most organic compounds inhibit corrosion via adsorption on the metal surface. The adsorption of these molecules depends mainly on certain physicochemical properties of the inhibitor molecule such as functional groups, steric factors, aromaticity, electron density at the donor atoms and π orbital character of donating electrons [16, 17], the electronic structure of the molecules [18, 19], and so on.

✉ O. Fergachi
omarfergachi@yahoo.fr

1 Laboratory of Materials Engineering and Environment: Modeling and Application, Faculty of Science, University Ibn Tofail, PB 133, Kenitra, Morocco

2 Laboratory Agro-Resources, Polymers and Process Engineering, Department of Chemistry, Faculty of Sciences, Ibn Tofail University, PO Box 133, 14000 Kénitra, Morocco

3 Laboratory of Materials, Electrochemistry and Environment, Faculty of Science, Ibn Tofail University, PB 133, Kenitra, Morocco

4 Regional Center for Education and Training, Allal AlFassi Avenue, Madinat AlIrfane, BP6210, Rabat, Morocco

5 Laboratory of separation processes, Faculty of Science, University Ibn Tofail, Kenitra, Morocco

In this study, we will focus on the efficiency of non-toxic imidazole derivatives as iron corrosion inhibitors in hydrochloric acid and, indeed, the corrosion inhibiting behavior of (2(-4(chloro phenyl-1*H*-benzo[d]imidazol)-1-yl)) phenylmethanone on ordinary iron in 5 M HCl solution. The aim of this work is devoted to study the inhibition characteristics of this compound for acid corrosion of ordinary steel using both potentiodynamic polarization and electrochemical impedance spectroscopy (EIS). The impedance spectra obtained from this study are analyzed to show the equivalent circuit that fits the corrosion data, also the adsorption behavior of these series is examined. In addition, Correlation between the quantum chemical calculations and molecular structure was discussed using density functional theory (DFT).

2 Experimental Procedure

2.1 Materials

Corrosion tests were performed on ordinary steel which had the following chemical composition by wt % (the rest is ordinary steel balance): C 0.11, Si 0.24, Mn 0.47, Cr 0.12, Mo 0.02, Ni 0.10, Al 0.03, Cu 0.14, Co < 0.0012, V < 0.003, W0.06. The steel specimens used have a rectangular form of 4.0 cm × 1.0 cm × 0.05 cm. The specimen's surface was prepared by polishing with emery paper at different grit sizes (from 60 to 1200), rinsing with distilled water, degreasing in ethanol, and drying at hot air. The aggressive solution of 5.0 M HCl was prepared by dilution of analytical grade 35% HCl with distilled water. Our inhibitory molecule is shown in Fig. 1.

2.2 Electrochemical Cell and Methods

2.2.1 Potentiodynamic Polarization Measurement

The working electrode was pressure-fitted into (2(-4(chloro phenyl-1*H*-benzo[d]imidazol)-1-yl)phenyl)methanone (CBIPM) exposing only 1 cm^2 of area to the solution.

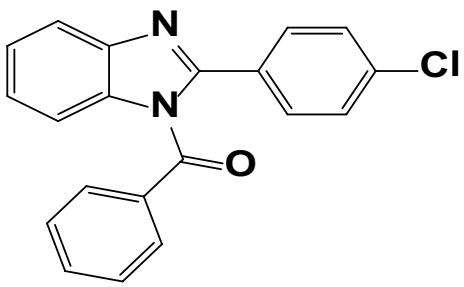

Fig. 1 Chemical structure of (2-(-4(chloro phenyl-1*H*-benzo[d] imidazol)-1-yl)phenyl)methanone (CBIPM)

Platinum and saturated calomel were used as counter and reference electrode (SCE), respectively.

These three electrodes are connected with the potentiostat/galvanostat (P G Z100) related to a computer with analysis software model (Volta master 4). The latter will display the results, namely the Tafel curves and electrochemical impedance diagrams. The ordinary steel was emerged in different concentrations of the test solution during 25 min stabilizing the electrochemical system until a steady-state of the open circuit potential (Eocp).

The potentiodynamic polarization curves were recorded by changing the electrode potential automatically from negative values to greater ones versus E_{corr} (from − 900 to − 100 mV/SCE) using a potentiostat/galvanostat type PGZ 100, at a scan rate of 1 mV/s.

The test solution was thermostatically controlled at ordinary temperature in air atmosphere. The corrosion inhibition efficiency is evaluated from the corrosion current densities values using the relationship:

$$\eta_{pp}\% = \left[\left(i^0_{corr} - i_{corr} \right) / i^0_{corr} \right] \times 100 \quad (1)$$

$$\theta = \left[\left(i^0_{corr} - i_{corr} \right) / i^0_{corr} \right], \quad (2)$$

where i^0_{corr} and i_{corr} are the corrosion current densities values without and with inhibitor, respectively. And θ *is* surface coverage.

2.2.2 Electrochemical Impedance Spectroscopy Measurements (EIS)

The electrochemical impedance spectroscopy measurements are carried out using a transfer function analyzer PGZ100 electrochemical system (Voltalab PGZ100, Radiometer Analytical), over the frequency range from 100 to 0.1 Hz with 10 points per decade. The applied amplitude of AC signal is 10 mV/ms. All experiments are performed at the open circuit potential. The obtained impedance data are analyzed in term of equivalent electrical circuit using Bouckamp's program [20].

The inhibiting efficiency derived from EIS (η_{imp}) is also added in Table 2 and calculated using the following equation:

$$\eta_{imp}\% = \frac{R_{ct} - R^0_{ct}}{R_{ct}} \times 100, \quad (3)$$

where R^0_{ct} and R_{ct} are the polarization resistance values in the absence and the presence of inhibitor, respectively.

2.3 UV–Visible Spectroscopy

Spectrophotometric method was carried out on the prepared ordinary steel samples after immersion in 5 M HCl with and without addition of 10^{-3} M of CBIPM at 298 K for 8 days. All the spectra measurements were carried out using a Beckman DU640 UV/Vis spectrophotometer.

2.4 Quantum Chemical Calculations

Theoretical calculations of the investigated molecules were performed in order to determine a relationship between some quantum chemical parameters obtained from the structure of our compound and the inhibition efficiencies of corrosion obtained experimentally [21, 22]. In this purpose, we have adopted the DFT (B3LYP) method using the 6-31G basis (d, p), and the calculation is done using a Gaussian software 09W [23–25]. The geometric optimization of the CBIPM inhibitor was carried out in the gaseous phase.

The various molecular quantum parameters such as electronegativity (χ), electronic affinity (A), ionization potential (I), and gap energy (ΔE_{gap}) are expressed by the following relations [26–29]:

$$\Delta E_{gap} = E_{LUMO} - E_{HOMO} \tag{4}$$

$$A = -E_{LUMO} \tag{5}$$

$$I = -E_{HOMO} \tag{6}$$

$$\chi = \frac{I + A}{2}, \tag{7}$$

where E_{HOMO} is the energy of the highest occupied molecular orbital and E_{LUMO} is the energy of the lowest vacant molecular orbital.

The overall hardness η and the chemical softness σ are given by the following equations [30]:

$$\eta = \frac{\Delta E_{gap}}{2} \tag{8}$$

$$\sigma = \frac{1}{\eta}. \tag{9}$$

The global electrophile index ω was introduced by Parr [31] and is given by

$$\omega = \frac{\mu^2}{2\eta}, \tag{10}$$

where μ is the electronic chemical potential, such as $\mu = -\chi^2$.

This index measures the propensity of chemical species to accept electrons. A good more reactive nucleophile is characterized by a lower value of μ, ω.

The number of transferred electrons (ΔN) was calculated as follows [32]:

$$\Delta N = \frac{\chi_{Fe} - \chi_{inh}}{2\left(\eta_{Fe} + \eta_{inh}\right)}, \tag{11}$$

where χ_{Fe} and $\chi_{inh,}$ respectively, represent the absolute electronegativity of iron and the inhibitor molecule, η_{Fe} and η_{inh} denote, respectively, the absolute hardness of iron and the molecule of inhibitor. The theoretical value of $\chi_{Fe} = 7.0$ eV and $\eta_{Fe} = 0$ is used to calculate the number of electrons transferred [33].

3 Results and Discussion

3.1 Concentration Effect

3.1.1 Tafel Polarization Study

Figure 2 shows anodic and cathodic polarization plots recorded on ordinary steel electrode in 5 M HCl in the absence and presence of different concentrations of CBIPM inhibitor. Electrochemical corrosion parameters, such as corrosion potential E_{corr} (mV/SCE), cathodic β_c Tafel slope (mV/dec), the corrosion current density i_{corr} (μA cm^{-2}), and inhibition efficiency η_{PP} (%), are given in Table 1.

It is clear from Fig. 2 that the addition of the CBIPM reduces both the cathodic and the anodic currents and therefore hinders the acid attack of the mild steel electrode in 5.0 M HCl. The cathodic Tafel curves obtained in Fig. 2

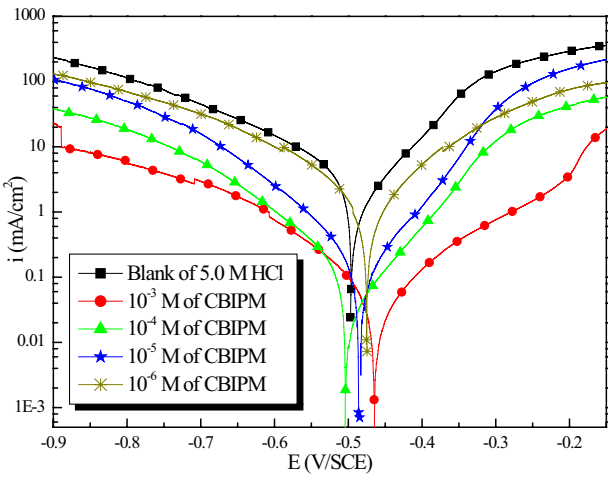

Fig. 2 Potentiodynamic polarization curves of ordinary steel in 5.0 M HCl solution containing different concentrations of CBIPM at 298 K

Table 1 Electrochemical parameters of ordinary steel in 5.0 M HCl solution in the absence and presence of different concentrations of CBIPM

Compounds	Conc. (M)	E_{corr} (mV/SCE)	i_{corr} (μA cm^{-2})	β_c (mV dec^{-1})	β_a (mV dec^{-1})	Θ	η_{PP} (%)
HCl 5.0 M	–	−494	4429	−202	92	–	–
CBIPM	10^{-3}	−462	62	−136	86	0.986	98.6
	10^{-4}	−502	87	−129	73	0.980	98
	10^{-5}	−484	163	−120	67	0.963	96.3
	10^{-6}	−472	1020	−104	79	0.769	76.9

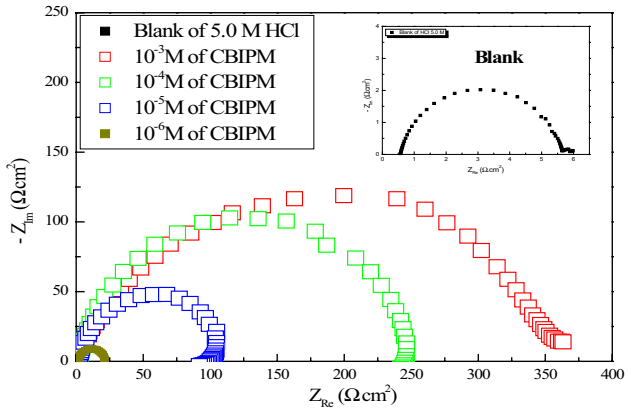

Fig. 3 Nyquist plots for ordinary steel in 5.0 M HCl solution in the absence and presence of different concentrations of CBIPM

indicate that the hydrogen evolution is activation-controlled and the reduction mechanism is not affected by the presence of inhibitor [34]. The inhibitor molecule is first adsorbed on the ordinary steel surface and blocking the available reaction sites.

From Table 1, it is clear that the i_{corr} values decrease considerably with the increase of the concentration of CBIPM. Accordingly, η_{PP} (%) values increase with increasing the inhibitor concentration reaching a maximum value of 98.6% with 10^{-3} M of CBIPM.

So, the high inhibition efficiency for CBIPM was attributed to the presence of electron donor groups *Chloro phenyl* in their structure. The adsorption of CBIPM on the metal surface can occur either directly on the basis of donor–acceptor interactions between the π-electrons of the ring and the vacant d-orbital of ordinary steel surface atoms or an interaction of organic nitrogen compounds with already adsorbed groups as proposed in the literature [35].

As shown in Table 1, the corrosion potential values were comparable, with the variation in E_{corr} between the absence and presence of the inhibitor being < 85 mV, thus allowing the inhibitor to be defined as a mixed type inhibitor [36, 37].

3.1.2 Electrochemical Impedance Spectroscopic Studies

The corrosion behavior of mild steel in 5.0 M HCl solution in the absence and presence of different concentrations of CBIPM is also investigated by EIS method at E_{corr} and at 298 K after 30 min of immersion. The representative Nyquist plots is shown in Fig. 3 and its extracted parameters are presented in Table 2. It is noted that the Nyquist plot of ordinary steel in the absence and presence of inhibitor contains a slightly depressed semi-circular shape and only one time constant appeared indicating that the ordinary steel corrosion is mainly controlled by a charge transfer process. In this case, the equivalent electric circuit, showed in Fig. 4 with one time constants was proposed to reproduce these results by non-linear regression calculation. However, it is seen that the R_{ct} values increased and C_{dl} values decreased with inhibitor concentration. These can be due to the decrease in local dielectric constant and/or increase in thickness of the electrical double layer, suggesting that CBIPM acts via adsorption at the metal/solution interface [38, 39].

Fig. 4 Electrical equivalent circuits used for modeling the metal/solution interface

Table 2 Electrochemical data of EIS for ordinary steel in 5.0 M HCl in the absence and presence of different concentrations of CBIPM

Inhibitor	C (M)	R_s (Ω cm^2)	R_{ct} (Ω cm^2)	C_{dl} (μF cm^{-2})	n_{dl}	Q (μF S^{n-1})	η_{imp} (%)
HCl	00	0.55	5	127	0.858	359	–
CBIPM	10^{-3}	6.79	362.7	27.97	0.770	80.3	98.6
	10^{-4}	2.4	245	71.35	0.903	105.6	97.9
	10^{-5}	1.4	106.5	67.36	0.902	108.8	95.3
	10^{-6}	1.3	21.4	73.45	0.955	98.8	76.6

Double layer capacitance values were obtained at maximum frequency (f_{max}) at which the imaginary component of the Nyquist plot is maximum and calculated using the following equation [40]:

$$C_{dl} = \frac{1}{2\pi f_{max} R_{ct}}. \quad (12)$$

3.2 Effect of Temperature

The study of the effect of temperature on the corrosion rate and inhibition efficiency facilitates the calculation of kinetic and thermodynamic parameters for the inhibition and the adsorption processes. These parameters are useful in interpreting the type of adsorption by the inhibitor. To calculate the activation energies and to investigate the mechanism of inhibition of the corrosion process, potentiodynamic polarization measurement (Figs. 5, 6) was taken at various temperatures in the presence and absence of 10^{-3} M of CBIPM. The related electrochemical parameters are presented in Table 3. This table represents the variation of current densities (i_{corr}) of ordinary steel corrosion in 50.0 M HCl in the absence and presence of optimum concentration of the studied compound at different temperatures (298–328 K).

The results show that i_{corr} in acid medium increases with increasing solution temperature, while the IE% decreases remarkably in the range of the studied temperature for acid medium, which is attributed to increase in the kinetic energy and decrease in the adsorption ability of organic compound at elevated temperature [41].

The activation parameters for the corrosion process were calculated from Arrhenius-type plot according to the following equations [42]:

$$i_{corr} = Ae^{\frac{-E_a}{RT}} \quad (13)$$

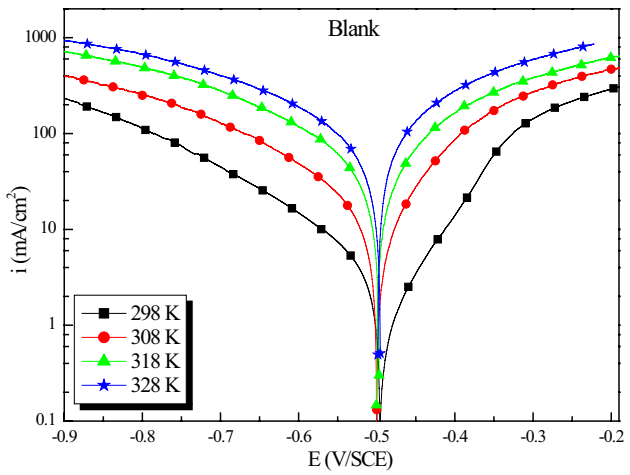

Fig. 5 Potentiodynamic polarization curves for ordinary steel in 5.0 M HCl at different temperatures without inhibitor

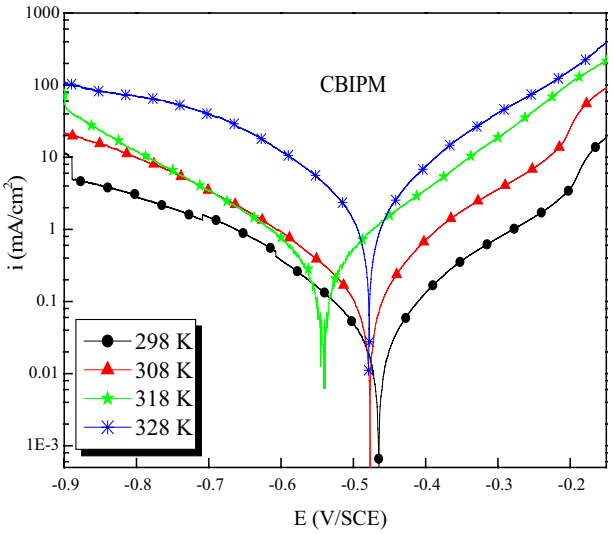

Fig. 6 Potentiodynamic polarization curves for ordinary steel in 5 M HCl with 10^{-3} M of CBIPM at different temperatures

$$\ln\left(\frac{i_{corr}}{T}\right) = \left[\ln\left(\frac{R}{hN_a}\right) + \left(\frac{\Delta S_a}{R}\right)\right] - \frac{\Delta H_a}{RT}, \quad (14)$$

where E_a is the apparent activation corrosion energy, A is the Arrhenius factor, h is the Plank's constant, N is the Avogadro's number, ΔH_a and ΔS_a are the enthalpy and the entropy changes of activation corrosion energies for the transition, respectively. R is the perfect gas constant.

The apparent activation energy was determined from the slopes of ln i_{corr} vs *1000/T* graph given in Fig. 7. A plot of ln (i_{corr}/T) against *1000/T* (Fig. 8) gave a straight line with slope ($\Delta H_a/R$) and intercept (ln(R/Nh) + ($\Delta S_a/R$)), from which the values of ΔH_a and ΔS_a were calculated and are listed in Table 4.

The increase in activation energy (E_a) of inhibited solutions compared to the blank solution suggests that inhibitor is physically adsorbed on the corroding electrode surface, whereas either unchanged or lower energy of activation in the presence of inhibitor suggests chemisorptions [43].

Inspection of these data reveals that the thermodynamic parameters ΔH_a and ΔS_a of dissolution reaction of ordinary steel in 5.0 M HCl in the presence of CBIPM are higher than in the absence of inhibitor. The positive sign of enthalpies reflect the endothermic nature of steel dissolution process meaning that dissolution of steel is difficult [44, 45]. The increase in E_a in the presence of CBIPM may be interpreted as chemical adsorption. This phenomenon suggested that a decrease in randomness occurred on going from reactants to the activated complex. The

Table 3 Electrochemical parameters of ordinary steel in 5 M HCl in the absence and presence of 10^{-3} M of CBIPM Mat different temperatures

Medium	Temperature	E_{corr} (mV/SCE)	I_{corr} (μA/cm²)	β_c (mv/dec)	β_a (mv/dec)	$E\%$
5.0 M HCl						
Blank (k)	298	−494	4429	−202	92	
	308	−499	6213	−189	99	
	318	−497	9179	−175	122	
	328	−496	16,923	−156	132	
10^{-3} M of CBIPM (k)	298	−462	62	−136	86	98.6
	308	−475	167	−154	153	97.3
	318	−536	358	−169	137	96
	328	−476	985	−165	143	94

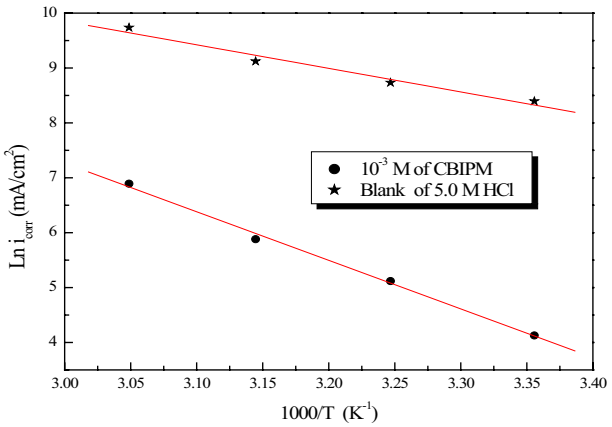

Fig. 7 Arrhenius plots of ordinary steel in 5.0 M HCl without and with 10^{-3} M of CBIPM

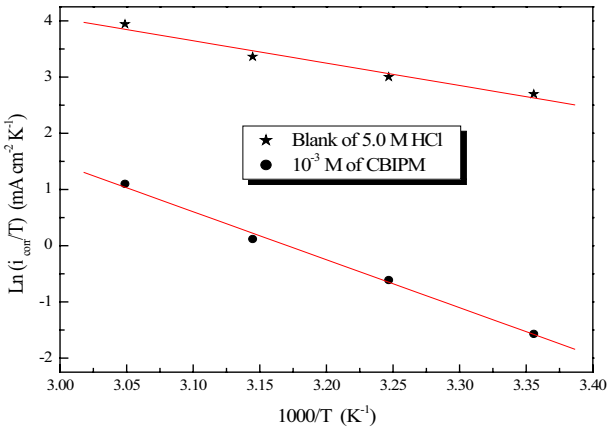

Fig. 8 Transition Arrhenius plots of ordinary steel in 5.0 M HCl in the absence and presence of CBIPM

great negative values of entropies indicate that the activated complex in the rate determining step is an association rather than dissociation step meaning that a decrease in disordering takes place on going from reactants to the activated complex [46, 47].

Table 4 The values of activation parameters E_a, ΔH_a, and ΔS_a for mild steel in 5.0 M HCl without and with different concentrations of CBIPM

Medium	E_a (KJ/mol)	ΔH_a (KJ/mol)	ΔS_a (KJ/mol)
Blank	35.68	33.09	−64.64
10^{-3} M of CBIPM	73.56	70.96	27.47

3.3 Adsorption Isotherm

The corrosion inhibition of metals as organic compounds was explained by their adsorption which possibly involves two types of interaction with metallic surface (physisorption, chemisorption). So, the adsorption process depends upon the charge and the nature of the metal surface, the chemical structure of inhibitor, and the electrolyte type [48]. Hence, the physisorption involves weak undirected interactions due to electrostatic attraction between inhibitor and the charge of metallic surface. However, the chemisorption process involves charge sharing or charge transfer from the inhibitor molecules to vacant d-orbitals of the metal surface in order to form a coordinate type bond [49].

However, several adsorption isotherms are usually used to describe the adsorption process, including Temkin, Frumkin, Parsons, and Flory–Huggins [50–53]. The best fit is obtained with the Langmuir isotherm. The Langmuir adsorption isotherm is given by [54]

$$\frac{C_{inh}}{\theta} = \frac{1}{K_{ads}} + C_{inh}, \tag{15}$$

where C_{inh} is the equilibrium inhibitor concentration and K_{ads} is the adsorptive equilibrium constant.

The plots of C_{inh}/θ against C_{inh} at different temperatures are presented in Fig. 9. They give the straight lines

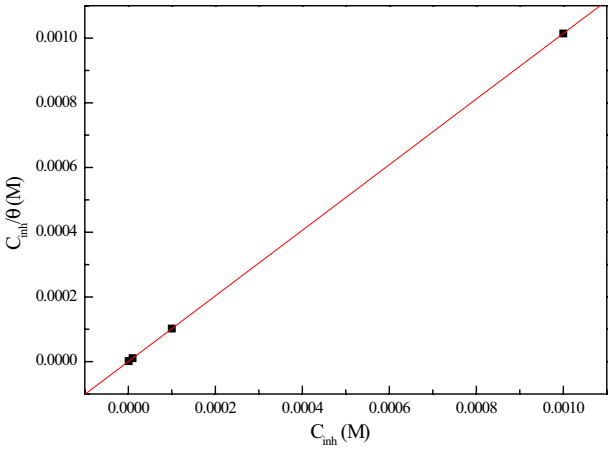

Fig. 9 Plot of Langmuir adsorption isotherm of CBIPM on the ordinary steel surface at 298 K

indicating the adsorption of CBIPM on ordinary steel surface obeys to the Langmuir adsorption isotherm.

Thermodynamic parameters including the heat of adsorption, free energy of adsorption, and entropy of adsorption are important in the explanation of the corrosion inhibition mechanism. The free energy of adsorption (ΔG_{ads}) can be obtained from the equation [55]:

$$K_{ads} = \left(\frac{1}{55.5}\right) \exp\left(-\frac{\Delta G^0_{ads}}{RT}\right), \quad (16)$$

where R is gas constant, T is absolute temperature of experiment, and the constant value of 55.5 is the concentration of water in solution in mol l^{-1}.

As it can be seen from Table 5, the addition of inhibitors causes negative values of ΔG_{ads}, indicating that adsorption of studied CBIPM is a spontaneous process [56]. It is generally accepted that when the values of ΔG_{ads} are greater than -20 kJ mol^{-1}, the type of adsorption is regarded as physisorption, the inhibition acts due to the electrostatic interactions between the charged molecules and the charged metal, while when values around -40 kJ mol^{-1} or lower, the type of adsorption is seen as chemisorption, which is due to the charge sharing or a transfer from the inhibitor molecules to the metal surface to form a covalent bond [57, 58]. The values of ΔG_{ads} in our measurements are -46.52 KJ/mol (Table 5), which suggests that the adsorption of CBIPM inhibitor involves a chemisorption interaction.

Table 5 Thermodynamic parameters for the adsorption of CBIPM on ordinary steel in 5.0 M HCl

Inhibitor	K_{ads} (L /mol)	ΔG_{ads} (KJ/mol)	R^2
10^{-3} of CBIPM	25×10^5	-46.52	1

3.4 UV–Visible Spectroscopy

A substantial support for the formation of metal complex is often obtained by UV–visible spectroscopic investigation. Since there is often a certain quantity of metal cation in the solution that is first dissolved from the metal surface, such procedures were conducted in the present work to confirm the possibility of the formation of [CBIPM-Fe^{2+}] complexes as described in the literature [59]. Furthermore, the change in position of the absorbance maximum and change in the value of absorbance indicate the formation of a complex between two species in solution [60]. In order to confirm the possibility of the formation of CBIPM-Fe complex, UV–visible absorption spectra obtained from 5.0 M HCl solution containing 10^{-3} M CBIPM before and after 6 days of ordinary steel immersion are shown in Fig. 10. The electronic absorption spectra of CBIPM before the steel immersion display a band of a high wavelength in the range of 200–340 nm due to the π–π* transition of aromatic ring of compound and a short band at around 500 and 520 nm which is attributed to a n–π* electronic transition involving the lone pair of electrons on the chlorophenyl benzo[d]imidazol nitrogen atom. After 6 days of steel immersion, it is evident that there is a remarkable translation of the curve to the right (from 340 to 400 nm) and it is clearly seen that the band in the region of 500–520 nm has been completely disappeared, indicating that the (*Chloro phenyl*) groups are strongly held up in the complex with Fe. In the mean time, there is an increase in the absorbance of this band. These experimental findings give strong evidence for the possibility

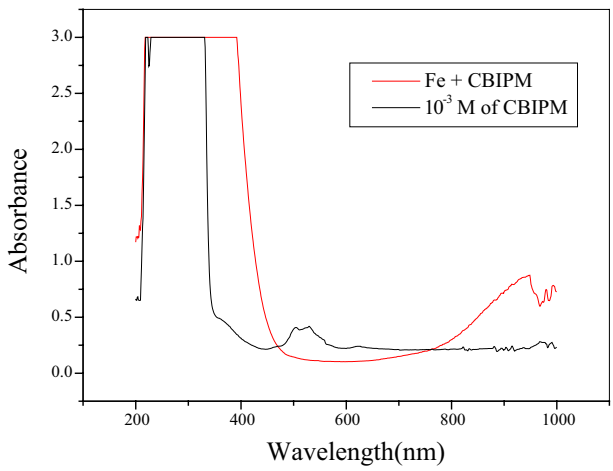

Fig. 10 UV–visible spectra of the solution containing 5.0 M HCl (10^{-3} Mol/l) CBIPM before (black) and after 6 days of ordinary steel immersion (red). (Color figure online)

of the formation of a complex between Fe^{2+} cation and CBIPM in HCl [61, 62].

3.5 Quantum Chemical Studies Using Density Functional Theory (DFT)

3.5.1 Calculation of the Main Quantum Parameters

The experimental study was completed by a theoretical study at the B3LYP/6-31G (d, p) level in order to correlate the results obtained from the experimental study with the structure and electronic properties of the inhibitor CBIPM. For this purpose, we will present the results of the theoretical study of the molecule CBIPM, which allowed us to identify a number of structural and electronic parameters of inhibitor used in this work such as the energy of the highest occupied molecular orbital (E_{HOMO}), the energy of the lowest unoccupied molecular orbital (E_{LUMO}), the energy gap between the HOMO and the LUMO (ΔE_{gap}), the ionization potential (I), electron affinity (A), dipole moment (μ), electronegativity (χ), global hardness (η), charge transfer rate (ΔN), and partial natural populations of Mulliken.

HOMO energy is often associated with the molecule's ability to give away its electrons to suitable vacant orbital. Thus, the HOMO high energy values of the inhibitor indicate its tendency to give electrons to an acceptor having an empty or vacant orbital molecular. The increase in E_{HOMO} values facilitates adsorption by influencing the transfer process through the adsorbed layer. On the other hand, LUMO gives information on the acceptance of electrons in the molecule. The decrease in the E_{LUMO} value is an indicator of the molecule's ability to accept electrons from the surface of iron. And as it is well known in the literature, a good corrosion inhibitor is often the one that not only yields its electrons but also capable of accepting the electrons of the metal surface; the lower the E_{LUMO} is, the higher the inhibitory efficiency is [63]. The adsorption performance between the inhibitors and the metal surface increases when ΔE_{gap} decreases because the energy to remove an electron from the lowest occupied orbital will be low [64]. Molecular optimization, electron density distributions of the boundary molecular orbitals, HOMO and LUMO of the CBIPM inhibitor are presented in Fig. 11. From Fig. 11, it can be seen that the electron density of the HOMO site is located on the chemical surface of the inhibitor (2-(4-chlorophenyl)-1*H*-benzo[d]imidazol-1-yl) CBIPM. On the other hand, the electron density of the unoccupied molecular orbital (LUMO) is distributed on the chemical surf of phenyl methanone of the inhibitor CBIPM. The calculated quantum parameters are summarized in the following Table 6.

The data grouped in Table 6 show that the CBIPM inhibitor has a high HOMO (− 5.981 eV) energy and a low LUMO energy (− 2.076 eV), as well as a low energetic difference value ΔE_{gap} (3.905 eV) between E_{HOMO} and E_{LUMO}, which reinforces its inhibitory action on the surface of the metal.

The dipole moment (μ) is the parameter most used to describe the polarity of a molecule [64]. It is defined as the charge product in the atom and the distance between two polar covalent bonds. However, the total dipole moment reflects only the global polarity of the molecule. It is clearly proved in the literature that molecules with high dipole moments are more reactive. In our study, the value of the dipole moment of CBIPM is 5.195 Debyes.

On the other hand, chemical hardness (η) and softness (σ) are important chemical properties for measuring molecular stability and reactivity; the results of these two parameters are also listed in Table 6. The inhibitory efficiency of adsorption of the inhibitor studied increases with chemical reactivity; normally the molecule with the smallest hardness value should have the greatest inhibition efficiency [66]. The CBIPM inhibitor has good chemical reactivity with the surface of the metal due to the increase in the softness value ($\sigma = 0.512\ eV^{-1}$) and the decrease in hardness ($\eta = 1.952$ eV).

The fraction of electrons transferred from the inhibitor molecule to the metal surface (ΔN) was also calculated in this work. According to the Lukovits study [67], if the value of $\Delta N < 3.6$, the inhibitory efficacy is judged to be good. In our case, the charge transfer rate is equal to $\Delta N = 0.761$ eV, and it is lower than the limit value set by Lukovits. It can be concluded that the inhibitor CBIPM has an inhibitory effect against corrosion of the metal.

3.5.2 Calculation of the Atomic Loads of Mulliken

It has been reported that the more negative the atomic charges of the adsorbed center are, the more easily the atom gives away its electrons to the unoccupied orbital of the metal [68]. The distribution of the Mulliken charges and the orientation of the polar moment are shown schematically in Fig. 12.

The values of the charges distribution are also grouped in Table 6.

From Fig. 12 and Table 7, it can be seen that the nitrogen, oxygen, and some carbon atoms have high charge densities. The regions of the greatest electronic densities are generally the sites where electrophiles can attack [69]. Thus, N, O, and some C atoms are the active centers that have the greatest ability to bind to the surface of the metal. On the other hand, some carbon atoms carry positive charges where nucleophiles can attack. Therefore, caffeine can accept iron electrons through these atoms, and these observations can be confirmed by the study of the Fukui indices.

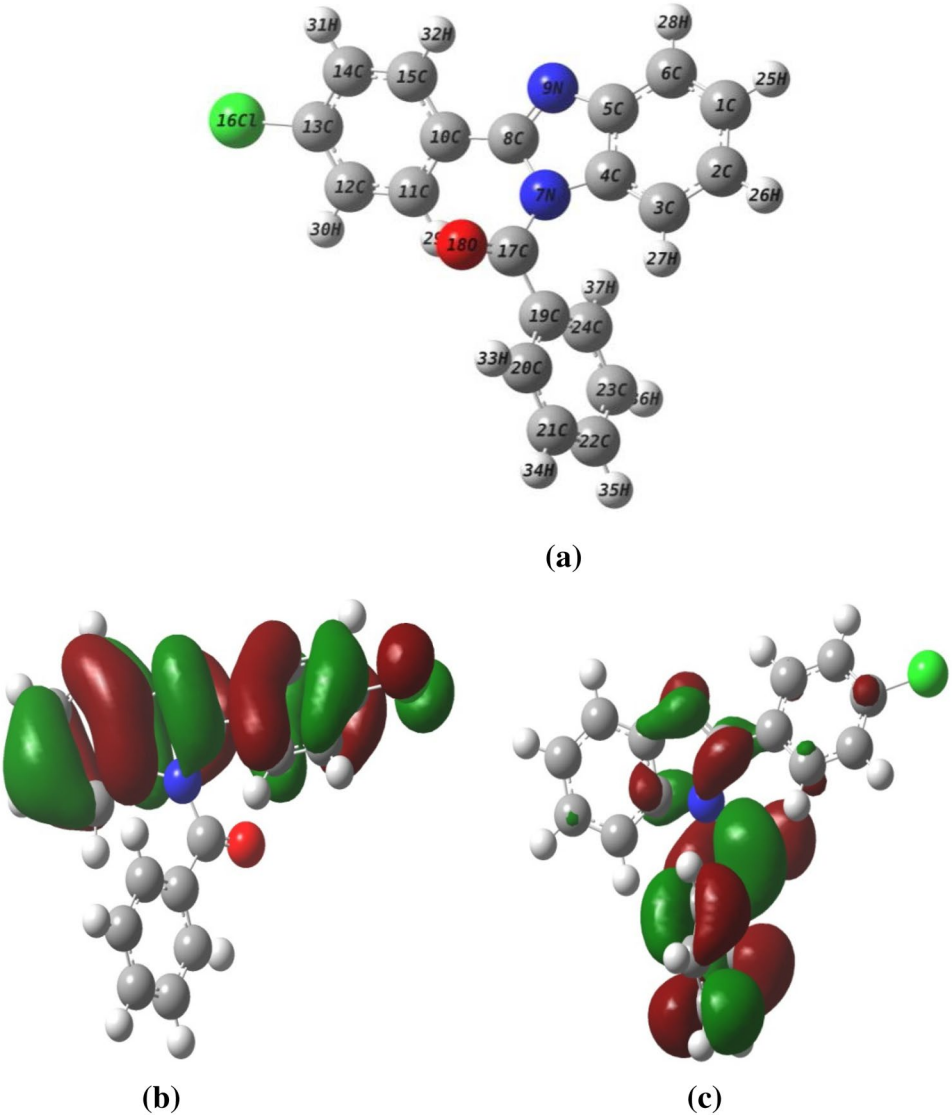

Fig. 11 Optimized molecular structure (**a**), HOMO (**b**) and LUMO (**c**) of the inhibitory molecule CBIPM using DFT/B3LYP/6-31 G (d, p)

Table 6 Calculated chemical quantum parameters of CBIPM

Parameters	E_{LUMO} (eV)	E_{HOMO} (eV)	ΔE_{gap} (eV)	μ (D)	η (eV)	σ (e V^{-1})	I (eV)	χ (eV)	A (eV)	ΔN	ω (eV)	TE (u.a)
CBIPM	− 2.076	− 5.981	3.905	5.195	1.952	0.512	5.981	4.028	2.076	0.761	3.904	− 1414.924

3.5.3 Study of the CBIPM Inhibitor's Local Reactivity by Using the Fukui Indices

The inhibitory molecules adsorb on the metal surfaces by donor–acceptor interactions. This means that it is essential to analyze the atoms in the molecule that participate in this type of interaction. The condensed form of Fukui functions in a molecule with N electrons has been proposed by Yang and Mortier [70]:

$$f_k^+ = P_k(N+1) - P_k(N) \quad \text{For nucleophilic attack} \tag{17}$$

$$f_k^- = P_k(N) - P_k(N-1) \quad \text{For electrophilic attack} \tag{18}$$

$P_k(N)$: Electronic population of the atom k in the neutral molecule.

$P_k(N+1)$: Electron population of the atom k in the anionic molecule.

$P_k(N-1)$: Electron population of the atom k in the cationic molecule.

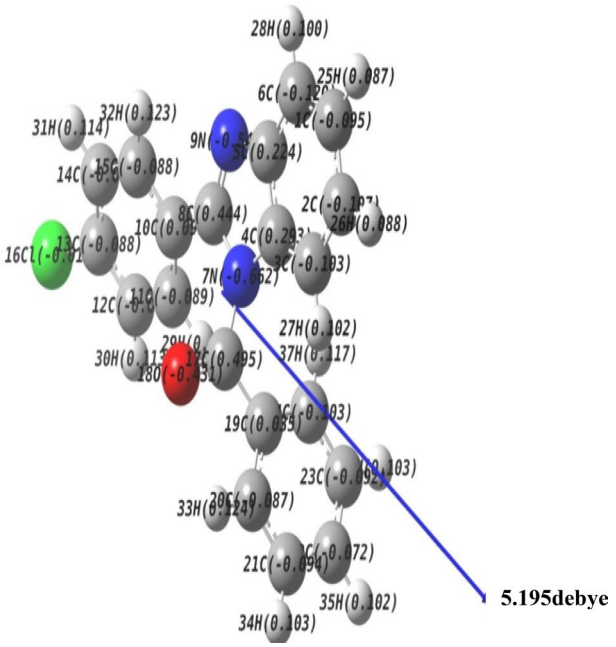

Fig. 12 Mulliken charge distribution of the CBIPM inhibitor

Table 7 Mulliken charge distribution of CBIPM inhibitor

Atoms	Mulliken charge distribution
C1	−0.094850
C2	−0.107059
C3	−0.103299
C4	0.293250
C5	0.223607
C6	−0.119657
N7	−0.661989
C8	0.444433
N9	−0.546838
C10	0.096984
C11	−0.088611
C12	−0.082625
C13	−0.088397
C14	−0.080751
C15	−0.087746
Cl16	−0.018677
C17	0.495385
O18	−0.430912
C19	0.034952
C20	−0.087133
C21	−0.094254
C 22	−0.071857
C23	−0.091643
C24	−0.102804

Table 8 Fukui indices calculated for the CBIPM inhibitors using DFT/B3LYP/6-31 G (d, p)

Inhibitor	Atoms	f_k^+	f_k^-
CBIPM	C1	0.011	0.016
	C2	0.01	0.050
	C3	−0.007	0.020
	C4	−0.004	0.041
	C5	0.006	0.028
	C6	0.012	0.032
	N7	−0.029	0.010
	C8	0.014	0.045
	N9	0.048	0.054
	C10	−0.010	0.014
	C11	−0.015	0.022
	C12	0.008	0.021
	C13	0.005	0.019
	C14	0.010	0.017
	C15	0.005	0.021
	Cl16	0.050	0.128
	C17	0.136	−0.007
	O18	0.131	0.017
	C19	0.002	−0.010
	C20	0.047	0.001
	C21	0.009	0.005
	C22	0.064	0.010
	C23	0.012	0.003
	C24	0.044	−0.012

Here f_k^+ and f_k^- represent the ability of the k atom to react with a nucleophile and electrophile, respectively. The high value of f_k^+ shows that the k atom has an electrophilic character indicating a high probability for a nucleophilic attack at that site. On the other hand, a high value of f_k^- means that the k-site is more nucleophilic and available for electrophilic attacks [71]. The calculated Fukui indices for the CBIPM inhibitor are shown in Table 8.

The results of Table 8 show that the CBIPM inhibitor possesses the greatest values of f_k^+, and these values are located on the atoms N9, C17, O18, C20, C22, and C24. These atoms participate in the acceptance of electrons from the metal surface. On the other hand, the atoms C2, C4, and Cl16 are electron donors as atoms possess higher f_k^- values. The theoretical results were found to be consistent with the experimental results of inhibition of metal corrosion by the CBIPM inhibitor.

4 Conclusion

The examined CBIPM is an effective corrosion inhibitor for ordinary steel in 5.0 M HCl solution. The potentiodynamic polarization curves indicated that these compounds act as mixed type inhibitors and their inhibition efficiencies increased with their concentrations to reach a maximum at 10^{-3} M. It is found also that the mechanism of the hydrogen reduction and the iron dissolution reactions change by the inhibitor addition. It acts by adsorption mechanism at the metallic surface and its inhibition depended on the nature of the N–H presented in their structures and the CBIPM compound is the best inhibitor. In addition, the inhibition efficiency decreased slightly with temperature. The thermodynamic study indicated that CBIPM can be acted by chemical adsorption at the metallic surface. The EIS measurements indicated that the plots were composed by one capacitive loop. The inhibition efficiencies of the studied compound were confirmed by all techniques' measurements. On the other hand, it was interesting to study the action mode of these compounds using UV–visible spectroscopy analysis techniques; it provided information about the nature of adsorption of CBIPM on the metallic surface. It could be interesting also to study the effect of these compounds on the corrosion of another metal in another acidic medium such as H_2SO_4 and H_3PO_4.

References

1. Amin MA, Khaled KF, Mohsen Q, Arida HA (2010) A study of the inhibition of iron corrosion in HCl solutions by some amino acids. Corros Sci 52(5):1684–1695.
2. Khaled KF (2003) The inhibition of benzimidazole derivatives on corrosion of iron in 1 M HCl solutions. Electrochim Acta 48(17):2493–2503.
3. El-Sayed A (1997) Phenothiazine as inhibitor of the corrosion of cadmium in acidic solutions. J Appl Electrochem 27(2):193–200.
4. Galai M, Rbaa M, Kacimi E, Ouakki Y, Dkhirech M, Touir N, Touhami R (2017) Anti-corrosion properties of some triphenylimidazole substituted compounds in corrosion inhibition of carbon steel in 1.0 M hydrochloric acid solution. Anal Bioanal Electrochem, 9(1), 80–101.
5. Barouni K, Kassale A, Albourine A, Jbara O, Hammouti B, Bazzi L (2014) Amino acids as corrosion inhibitors for copper in nitric acid medium: experimental and theoretical study. J Mater Environ Sci 5(2):456–463.
6. Schmitt G (1984) Application of inhibitors for acid media: report prepared for the European federation of corrosion working party on inhibitors. Br Corros J 19(4):165–176.
7. El-Rehim SA, Ibrahim MA, Khaled KF (1999) 4-Aminoantipyrine as an inhibitor of mild steel corrosion in HCl solution. J Appl Electrochem 29(5):593–599.
8. Li XH, Deng SD, Fu H (2011) Adsorption and inhibitive action of hexadecylpyridinium bromide on steel in phosphoric acid produced by dihydrate wet method process. J Appl Electrochem 41(5):507–517.
9. Ech-chihbi E, Salim R, Oudda H, Elaatiaoui A, Rais Z, Oussaid A, Taleb M (2016) Effect of some imidazopyridine compounds on carbon steel corrosion in hydrochloric acid solution. Der Pharm Chem 8(13):214–230.
10. Ech-chihbi E, Belghiti ME, Salim R, Oudda H, Taleb M, Benchat N, El-Hajjaji F (2017) Experimental and computational studies on the inhibition performance of the organic compound "2-phenylimidazo [1,2-a]pyrimidine-3-carbaldehyde" against the corrosion of carbon steel in 1.0 M HCl solution. Surf Interf 9:206–217.
11. Dkhireche N, Galai M, Kacimi E, Rbaa Y, Ouakki M, Lakhrissi M, Ebn B, Touhami M (2018) New quinoline derivatives as sulfuric acid inhibitor's for mild steel. Anal Bioanal Electrochem 10(1):111–135.
12. Rbaa M, Galai M, Kacimi E, Ouakki Y, Touir M, Lakhrissi R, Touhami B, M. E (2017) Adsorption properties and inhibition of carbon steel corrosion in a hydrochloric solution by 2-(4,5-diphenyl-4,5-dihydro-1*H*-imidazol-2-yl)-5-methoxyphenol. Portug Electrochim Acta 35(6):323–338.
13. Alaoui K, Touir R, Galai M, Serrar H, Ouakki M, Kaya S, El Kacimi Y (2018) Electrochemical and computational studies of some triazepine carboxylate compounds as acid corrosion inhibitors for mild steel. J Bio Tribo Corr 4(3):37.
14. Kertit S, Hammouti B (1996) Corrosion inhibition of iron in 1 M HCl by 1-phenyl-5-mercapto-1,2,3,4-tetrazole. Appl Surf Sci 93(1):59–66.
15. Essoufi H, Kertit S, Hammout B, Benkaddour M (2000) 1-Phenyl-5-mercapto-1,2,3,4-tetrazole (PMT) as corrosion inhibitor for nickel in sulphuric acid solution. Bull Electrochem 16(5):205–208.
16. Growcock FB, Frenier WW, Andreozzi PA (1989) Inhibition of steel corrosion in HCl by derivatives of cinnamaldehyde: Part II. Structure–activity correlations. Corrosion 45(12):1007–1015.
17. Lukovits I, Kalman E, Palinkas G (1995) Nonlinear group-contribution models of corrosion inhibition. Corrosion 51(3):201–205.
18. Bentiss F, Lagrenee M, Traisnel M, Mernari B, Elattari H (1999) A simple one step synthesis of new 3,5-disubstituted-4-amino-1,2,4-triazoles. J Heterocyclic Chem 36(1):149–152.
19. Bentiss F, Lagrenee M, Traisnel M, Hornez JC (1999) The corrosion inhibition of mild steel in acidic media by a new triazole derivative. Corros Sci 41(4):789–803.
20. Bouckamp A, Users manual equivalent circuit, Ver. 4.51 (1993).
21. El Hezzat M, Assouag M, Zarrok H, Benzekri Z, El Assyry A, Boukhris S, Oudda H (2015) Correlated DFT and electrochemical study on inhibition behavior of ethyl 6-amino-5-cyano-2-methyl-4-(p-tolyl)-4*H*-pyran-3-carboxylate for the corrosion of mild steel in HCl. Der Pharm Chem 7(10):77–88.
22. El Aoufir Y, Lgaz H, Bourazmi H, Kerroum Y, Ramli Y, Guenbour A, Oudda H (2016) Quinoxaline derivatives as corrosion inhibitors of carbon steel in hydrochloridric acid media: electrochemical, DFT and Monte Carlo simulations studies. J Mater Environ Sci 7(12):4330–4347.
23. Frisch MJ, Trucks GW, Schlegel HB, Scuseria GE, Robb MA, Cheeseman JR, Millam JM (2003) Gaussian 03, Revision B. 03. Gaussian, Pittsburgh.
24. Petersson A, Bennett A, Tensfeldt TG, Al-Laham MA, Shirley WA, Mantzaris J (1988) A complete basis set model chemistry. I. The total energies of closed-shell atoms and hydrides of the first-row elements. J Chem Phys 89(4):2193–2218.
25. Ansari KR, Quraishi MA (2015) Experimental and quantum chemical evaluation of Schiff bases of isatin as a new and green corrosion inhibitors for mild steel in 20% H_2SO_4. J Taiwan Inst Chem Eng 54:145–154.
26. Neese F (2012) An Ab ini tio, DFT and semiempirical SCF-MO package. Max-Plank Institute for Bioinorganic Chemistry, Mülheim ad Ruhr.

27. Becke AD (1986) Density functional calculations of molecular bond energies. J Chem Phys 84(8):4524–4529.
28. Lee C, Yang W, Parr RG (1988) Development of the Colle–Salvetti correlation-energy formula into a functional of the electron density. Phys Rev B 37(2):785.
29. Saha SK, Hens A, RoyChowdhury A, Lohar AK, Murmu NC, Banerjee P (2014) Molecular dynamics and density functional theory study on corrosion inhibitory action of three substituted pyrazine derivatives on steel surface. Can Chem Trans 2(4):489–503.
30. Saha SK, Ghosh P, Hens A, Murmu NC, Banerjee P (2015) Density functional theory and molecular dynamics simulation study on corrosion inhibition performance of mild steel by mercaptoquinoline Schiff base corrosion inhibitor. Phys E 66:332–341.
31. Chermette H (1999) Chemical reactivity indexes in density functional theory. J Comput Chem 20(1):129–154.
32. Pearson RG (1988) Absolute electronegativity and hardness: application to inorganic chemistry. Inorg Chem 27(4):734–740.
33. Parr RG, Pearson RG (1983) Absolute hardness: companion parameter to absolute electronegativity. J Am Chem Soc 105(26):7512–7516.
34. Lukovits I, Kalman E, Zucchi F (2001) Corrosion inhibitors—correlation between electronic structure and efficiency. Corrosion 57(1):3–8.
35. Shukla SK, Quraishi MA (2009) 4-Substituted anilinomethylpropionate: new and efficient corrosion inhibitors for mild steel in hydrochloric acid solution. Corros Sci 51(9):1990–1997.
36. Benali O, Larabi L, Traisnel M, Gengembre L, Harek Y (2007) Electrochemical, theoretical and XPS studies of 2-mercapto-1-methylimidazole adsorption on carbon steel in 1 M $HClO_4$. Appl Surf Sci 253(14):6130–6139.
37. Quraishi MA, Rawat J (2000) Corrosion inhibition of mild steel in acid solutions by tetramethyl-dithia-octaazacyclotetradeca hexaene (MTAT). Anti Corr Methods Mater 47(5):288–293.
38. Lagrenee M, Mernari B, Bouanis M, Traisnel M, Bentiss F (2002) Study of the mechanism and inhibiting efficiency of 3,5-bis(4-methylthiophenyl)-4*H*-1,2,4-triazole on mild steel corrosion in acidic media. Corros Sci 44(3):573–588.
39. El Makrini B, Larouj M, Lgaz H, Salghi R, Salman A, Belkhaouda M, Oudda H ISSN 0975-413X CODEN (USA): PCHHAX.
40. El Makrini B, Lgaz H, Larouj M, Salghi R, Hasan AR, Belkhaouda M, Oudda H (2016) The inhibition performance of sulfamerazine for corrosion of mild steel in HCl. Der Pharma Chem 8(2):256–268.
41. Tsuru T, Haruyama S, Gijutsu B (1978) Corrosion inhibition of iron by amphoteric surfactants in 2 M HCl. J Jpn Soc Corros Eng 27:573–581.
42. Tang Y, Zhang F, Hu S, Cao Z, Wu Z, Jing W (2013) Novel benzimidazole derivatives as corrosion inhibitors of mild steel in the acidic media. Part I: gravimetric, electrochemical, SEM and XPS studies. Corr Sci 74:271–282.
43. Hegazy MA, Badawi AM, Rehim E, Kamel SA, W. M (2013) Corrosion inhibition of carbon steel using novel *N*-(2-(2-mercaptoacetoxy) ethyl)-*N,N*-dimethyl dodecan-1-aminium bromide during acid pickling. Corros Sci 69:110–122.
44. Shivakumar SS, Mohana KN (2013) Corrosion behavior and adsorption thermodynamics of some Schiff bases on mild steel corrosion in industrial water medium. Int J Corr 2013:8207.
45. Methal A, Koulou A, El Bakri M, Touhami ME, Galai M, Lakhrissi M, Bakkali S Green approach to corrosion inhibition of mild steel in 1 M HCl solutions by Monosaccharides derivatives. Maghreb J Pure Appl Sci 1(2), 46–61.
46. Oguzie EE (2007) Corrosion inhibition of aluminium in acidic and alkaline media by Sansevieria trifasciata extract. Corr Sci 49(3):1527–1539.
47. Martinez S, Stern I (2002) Thermodynamic characterization of metal dissolution and inhibitor adsorption processes in the low carbon steel/mimosa tannin/sulfuric acid system. Appl Surf Sci 199(1–4):83–89.
48. Benabdellah M, Aouniti A, Dafali A, Hammouti B, Benkaddour M, Yahyi A, Ettouhami A (2006) Investigation of the inhibitive effect of triphenyltin 2-thiophene carboxylate on corrosion of steel in 2 M H_3PO_4 solutions. Appl Surf Sci 252(23):8341–8347.
49. Noor EA, Al-Moubaraki AH (2008) Thermodynamic study of metal corrosion and inhibitor adsorption processes in mild steel/1-methyl-4[4′(-X)-styryl pyridinium iodides/hydrochloric acid systems. Mater Chem Phys 110(1):145–154.
50. Subramanyam NC, Mayanna SM (1985) Azoles as corrosion inhibitors for mild steel in alkaline mine water. Corr Sci 25(3):163–169.
51. Eldakar N (1981) Ken Nobe. Corrosion 36:271.
52. Kurosawa K, Fukushima T (1989) Effects of pH of an Na_2MoO_4-H_3PO_4 type aqueous solution on the formation of chemical conversion coatings on steels. Corr Sci 29(9):1103–1114.
53. Kuznetsov YI (2001) Corrosion inhibitors in conversion coatings. III. Protect Metals 37(2):101–107.
54. Deng S, Li X, Fu H (2011) Acid violet 6B as a novel corrosion inhibitor for cold rolled steel in hydrochloric acid solution. Corros Sci 53(2):760–768.
55. Adardour L, Lgaz H, Salghi R, Larouj M, Jodeh S, Zougagh M, Taleb M (2016) Corrosion inhibition of steel in phosphoric acid by sulfapyridine experimental and theoretical studies. Der Pharm Lett 8(4):173–185.
56. Migahed MA (2005) Electrochemical investigation of the corrosion behaviour of mild steel in 2 M HCl solution in presence of 1-dodecyl-4-methoxy pyridinium bromide. Mater Chem Phys 93(1):48–53.
57. Ahamad I, Prasad R, Quraishi MA (2010) Thermodynamic, electrochemical and quantum chemical investigation of some Schiff bases as corrosion inhibitors for mild steel in hydrochloric acid solutions. Corr Sci 52(3):933–942.
58. Ehteram A, Aisha H (2008) Thermodynamic study of metal corrosion and inhibitor adsorption processes in mild steel/1-methyl-4 [40(-X)-styryl pyridinium iodides/hydrochloric acid systems. Mater Chem Phys 110:145–154.
59. Abboud Y, Abourriche A, Saffaj T, Berrada M, Charrouf M, Bennamara A, Hannache H (2007) 2,3-Quinoxalinedione as a novel corrosion inhibitor for mild steel in 1 M HCl. Mater Chem Phys 105(1):1–5.
60. Goel R, Siddiqi WA, Ahmed B, Khan MS, Chaubey VM (2010) Synthesis characterization and corrosion inhibition efficiency of N-C2{(2E)-2-[4-(dimethylamino) benzylidene] hydrazinyl}2-oxo ethyl benzamide on mild steel. Desalination 263(1–3):45–57.
61. Alaa SA, Ayman A (2006) El-Fetouh. Gouda., Ragaa, El-Sheikh., Faten, Zahran. Spectrochim Acta A Mol Biomol Spectrosc 2006:14–171.
62. Anacona JR, Martell T, Sanchez I (2005) Metal complexes of a new ligand derived from 2,3-quinoxalinedithiol and 2,6-bis(bromomethyl)pyridine. J Chil Chem Soc 50(1):375–378.
63. Efil K, Bekdemir Y (2015) Theoretical study on corrosion inhibitory action of some aromatic imines with sulphanilic acid: A DFT study. Can Chem Trans 3(1):85–93.
64. Wang H, Wang X, Wang H, Wang L, Liu A (2007) DFT study of new bipyrazole derivatives and their potential activity as corrosion inhibitors. J Mol Model 13(1):147–153.
65. Yıldız R (2015) An electrochemical and theoretical evaluation of 4,6-diamino-2-pyrimidinethiol as a corrosion inhibitor for mild steel in HCl solutions. Corros Sci 90:544–553.

66. Al Hamzi AH, Zarrok H, Zarrouk A, Salghi R, Hammouti B, Al-Deyab SS, Guenoun F (2013) The role of acridin-9(10*H*)-one in the inhibition of carbon steel corrosion: thermodynamic, electrochemical and DFT studies. Int J Electrochem Sci 8:2586–2605.
67. Ramya K, Mohan R, Joseph A (2014) Adsorption and electrochemical studies on the synergistic interaction of alkyl benzimadazoles and ethylene thiourea pair on mild steel in hydrochloric acid. J Taiwan Inst Chem Eng 45(6):3021–3032.
68. Al-Azawi KF, Al-Baghdadi SB, Mohamed AZ, Al-Amiery AA, Abed TK, Mohammed SA, Mohamad AB (2016) Synthesis, inhibition effects and quantum chemical studies of a novel coumarin derivative on the corrosion of mild steel in a hydrochloric acid solution. Chem Cent J 10(1):23.
69. Obi-Egbedi NO, Essien KE, Obot IB, Ebenso EE (2011) 1,2-Diaminoanthraquinone as corrosion inhibitor for mild steel in hydrochloric acid: weight loss and quantum chemical study. Int J Electrochem Sci 6:913–930.
70. Özcan M, Dehri I, Erbil M (2004) Organic sulphur-containing compounds as corrosion inhibitors for mild steel in acidic media: correlation between inhibition efficiency and chemical structure. Appl Surf Sci 236(1–4):155–164.
71. Yang W, Mortier WJ (1986) The use of global and local molecular parameters for the analysis of the gas-phase basicity of amines. J Am Chem Soc 108(19):5708–5711.